ISSN: 2579-5821 (Print)
ISSN: 2579-5546 (Online)
URL address: http://journal.unhas.ac.id/index.php/geocelebes
DOI: 10.20956/geocelebes.v7i2.23759

Jurnal Geocelebes Vol. 7 No. 2 October 2023, 117 – 129

Identification of Mount Sirung Geothermal Potential based on Land Surface Temperature and 3D Gravity Model

Ayu Alvita Primastika[1]*, Dhika Faiz Fadrian[2], Fardhan Rafshan Zani[2], Nanda Ridki Permana[3]

[1]GeoXplore Indonesia, Kincir Air Street, Pondok Manggis Block B6, Bojong Baru, Bojonggede, Bogor, West Java, 16920, Indonesia.
[2]Department of Physics, Faculty of Science and Technology, Syarif Hidayatullah State Islamic University Jakarta, 95 Ir. H. Juanda Street, Cempaka Putih, Ciputat, South Tangerang, Banten, 15412, Indonesia.
[3]PT Minelog Services Indonesia, Bumi Serpong Damai (BSD), Industrial Estate and Warehouse Techno Park Block G1 Number 10, Sector 11 Street, Setu, South Tangerang, Banten, 15220, Indonesia.

*Corresponding author. Email: ayu.alvitaa@gmail.com

Manuscript received: 24 November 2022; Received in revised form: 29 January 2023; Accepted: 31 January 2023

Abstract

According to the Ministry of Energy and Mineral Resources 2021 data, first ranks in the list of 10 provinces with the lowest electrification ratio in Indonesia. One of the geothermal prospect areas in East Nusa Tenggara is Mount Sirung. This research was conducted in August 2022 which aims to identify geothermal systems. Gravity data was obtained from the GGMPlus 2013 with a total of 3819 data. Land Surface Temperature (LST) is used as supporting data with a surface temperature approximately 26.1 – 29.5°C because there are manifestations of hot springs at Mount Sirung. Based on the derivative analysis, there are four trajectories in the northwest-southeast direction with reverse faults and normal faults as the geothermal control system of Mount Sirung. The results of 3D gravitational inversion modeling are estimated that there is clay interspersed with breccia with a density of 2.34 – 2.39 g/cm^3 as clay cap at 0 – 600 m, and lava interspersed with sandy tuff as a reservoir with a density of 1.98 – 2.03 g/cm^3 at 700 – 1400 m. Based on these results and discussions, Mount Sirung is proven to have geothermal potential which can be utilized as a source of electrification in East Nusa Tenggara.

Keywords: derivative analysis; geothermal; gravity; Land Surface Temperature; Mount Sirung.

Citation: Primastika, A .A., Fadrian, D. F., Zani, F. R., and Permana, N. R. (2023). Identification of Mount Sirung Geothermal Potential based on Land Surface Temperature and 3D Gravity Model. *Jurnal Geocelebes*, 7(2), 117–129, doi: 10.20956/geocelebes.v7i2.23759

Introduction

Indonesia is a country that is crossed by the Ring of Fire so that it has a very large geothermal resource, covering about 40% of the world's potential or 29,544 MW. However, only about 7.2% is used as domestic electrical energy (Gunawan et al., 2021). Geothermal potential is shown by the existence of 117 active volcanoes scattered throughout the country, one of which is the East Nusa Tenggara area with a total potential of 980 Mwe spread over about 24 locations (Ministry of Energy and Mineral Resources, 2017).

East Nusa Tenggara ranks first in the list of 10 provinces with the lowest electrification ratio in Indonesia at 88.81% (Ministry of Energy and Mineral Resources, 2021). Therefore, the government is obliged to conduct a geothermal demand survey as one of the sources of geothermal power plants, especially in East Nusa Tenggara (Yudha et al., 2022).

One of the geothermal prospect areas in East Nusa Tenggara is Mount Sirung, located on Pantar Island at the eastern end of the Flores to Alor Island range. Mount Sirung has a hypothetical geothermal

resource of 45 Mwe. The manifestation of Mount Sirung consists of 4 hot springs located on a fault line with an average spring pH of 6.03 – 7.17 (Hadi & Kusnadi, 2015).

Research conducted by Wachidah & Minarto (2018) using the gravity method with derivative analysis shows that there is a northeast-southwest direction fault as a rock constituent of breccia tuff, lapilli tuff, tuff, dacite breccia, and andesite intrusion (Wachidah & Minarto, 2018). Another study conducted by Sidik et al. (2014) using the gravity method showed that there were three faults on three measurement tracks as an early indication of gold mineralization (Sidik et al., 2014). The mineralization process is the result of a chemical process between hydrothermal fluid and the rocks it passes through, so that primary minerals are converted into alteration minerals which can be an indication of geothermal prospect (Rey & Poluakan, 2020).

Based on the background and previous research, this study aims to analyze the geothermal potential of Mount Sirung based on surface temperature, the type of faults that control the geothermal system, and the subsurface structure of the geothermal manifestation of Mount Sirung using geophysical methods. One of the geophysical methods that can be used is the gravity method with derivative analysis correlated with Land Surface Temperature (LST) data.

Regional Geology of Mount Sirung

The lithology of Mount Sirung is composed of the Upper Miocene aged Alor Formation (Tmpa) in the form of lava, breccia, and coarse-grained passive tuff. Old volcanic rocks (Qtv) of Pleistocene age in the form of lavas, breccias, agglomerates, tuffs, volcanic sands, and rocky passive tuff. Coral limestone (Ql) and young volcanic rocks (Qhv) of Holocene age are lava, breccia, agglomerate, pebbles, sand, and volcanic ash (Koesoemadinata & Noya, 1969).

The geological structure at Mount Sirung (Figure 1) is a northeast-southwest trending fault with a distribution of volcanic rocks and limestone that overlies the overlying volcanic rocks. Another structure caused by volcanic processes is the caldera around the summit of Mount Sirung which forms a permeable zone where fluid accumulates as a geothermal prospect location (Sugianto et al., 2017; Rahadinata et al., 2019).

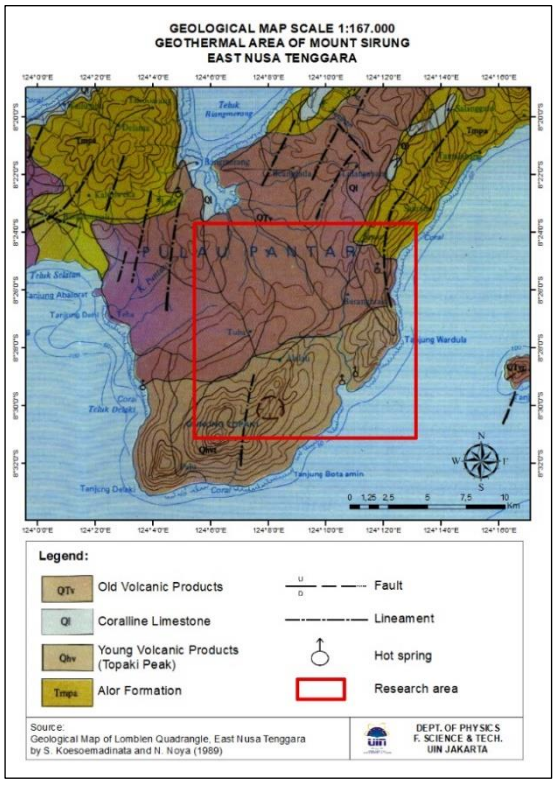

Figure 1. Geological map of Mount Sirung (Koesoemadinata & Noya, 1969).

Literature Review

Geothermal system is a system of heat in a certain volume that comes from magma kitchens, intrusion bodies, or heat due to earth's core pressure. The geothermal system component (Figure 2) consists of three main components, which is the presence of permeable reservoir rock, the presence of fluid that carries heat, and the heat source itself (Ashat et al., 2019). The freezing of magma as a heat source produces igneous rocks that conductively

flow heat to the surrounding rocks. The propagating heat heats the fluid in the reservoir (Luthfi et al., 2020). The fluid moves upward through the hot springs to the surface to meet the clay cap as a geothermal fluid trap (Sarkowi et al., 2021). Based on the geological structure, geothermal systems in Indonesia are divided into three, which are volcanic, volcanic-tectonic, and non-volcanic geothermal systems (Salam et al., 2017).

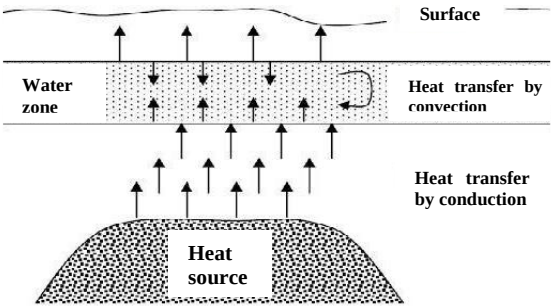

Figure 2. Water circulation or convection on geothermal system (Saptadji, 2001).

The gravity method is a method of measuring gravitational acceleration in the subsurface due to differences in rock density and differences in the earth's topography. The gravity method is based on Newton's II law:

$$F = G\frac{m_1 m_2}{r^2} \quad (1)$$

where F is the force on m_1 due to m_2 (Newton), G is the gravitational constant, m is the mass (kg), and r is the distance between m_1 and m_2 (m) (Imran et al., 2021).

Bouguer Correction (BC) is carried out to reduce the effect of gravity between the measurement point and the reference point, with the equation:

$$BC = 0.04193\ x\ \rho\ x\ h\ mGal/ft \quad (2)$$

where ρ is the Bouguer mass density (kg/m^3) and h is the height of the measurement point from the spheroid plane (m) (Sugita et al., 2020).

Free Air Correction (FAC) is performed due to altitude differences with the assumption that mass is concentrated at the center of the earth, with the equation:

$$FAC = 0{,}3086\ x\ h\ mGal \quad (3)$$

where h is the point height (m) (Sugita et al., 2020).

Terrain Correction (TC) is carried out because of the increase or decrease in measured gravity values due to irregular altitude, with the equation:

$$TC = \frac{0.04193}{n}\rho\left\{(r^2 - r^1) + \sqrt{r_1^2 + L^2} - \sqrt{r_2^2 + L^2}\right\} \quad (4)$$

where n is the number of compartments, r_1 is the inner radius (m), r_2 is the outer radius (m), and L is the height difference of measurement points (m) (Reynolds, 1997).

First Horizontal Derivative (FHD) is an analysis of the rate of change of horizontal gravity (mGal/m) based on the limit of gravity density contrast to show the geological structure of faults, with the equation:

$$\frac{\delta_g}{\delta_x}(x_n, y_n) = \sqrt{\left(\frac{\delta_g}{\delta_x}\right)^2 + \left(\frac{\delta_g}{\delta_y}\right)^2} \quad (5)$$

where $\left(\frac{\delta_g}{\delta_x}\right)^2$ and $\left(\frac{\delta_g}{\delta_y}\right)^2$ are the first derivative of gravity with respect to x and y data (Yulistina, 2018; Sehah et al., 2021).

Second Vertical Derivative (SVD) is a second derivative that can analyze shallow geological structures by interpreting the zero value as the outline of the rock body, with the equation:

$$\frac{\delta^2 \Delta g}{\delta z^2} = -\left(\frac{\delta^2 \Delta g}{\delta x^2} + \frac{\delta^2 \Delta g}{\delta y^2}\right) \quad (6)$$

where $g''_{max} > g''_{min}$ is the normal fault and $g''_{max} < g''_{min}$ is the reverse fault (Ibrahim et al., 2022; Permana et al., 2022a).

Land Surface Temperature (LST) is the average surface temperature controlled by the energy balance of atmosphere, material

emissivity, and thermal properties of the surface, with the equation:

$$T_S = \frac{BT}{\left\{1+\left[\left(\frac{\lambda BT}{\rho}\right) ln\, \varepsilon\lambda\right]\right\}} \quad (7)$$

where T_S is land surface temperature (°C), BT is brightness temperature (°C), λ is the emission wavelength, ε is emissivity, and ρ is spectral radiance (Imran et al., 2021).

Inversion modeling is an analysis process with a statistical approach in the form of curve matching between observational data and mathematical models (Hartini, 2020), with the equation:

$$m = F^{-1}(d) \quad (8)$$

where F is the operator associated with the model, m is the model calculation data, and d is the model observation data (Permana et al., 2022b). In this research, the inversion process is used to analyze the subsurface according to the results of the projection of the gravity anomaly of the research area.

Methods

The research was conducted in August 2022, with the research location at Mount Sirung, East Nusa Tenggara (9058450.00 m S – 9073207.00 m S and 621089.00 m E – 633540.00 m E) UTM 51 L zone (Figure 3) suspected of having geothermal manifestations (Ministry of Energy and Mineral Resources, 2017).

The data used is gravity satellite was obtained from the GGMPlus 2013. The amount of data used is 3819 data, consisting of gravity disturbance (gd), geoid, and Digital Elevation Model (DEM), corrected with gravity correction that produces Complete Bouguer Anomaly (CBA). Residual anomalies generated from anomaly separation are used to analyze fault types with derivative analysis in the form of First Horizontal Derivative (FHD) and Second Vertical Derivative (SVD) and for processing 3D inversion modeling of subsurface gravity data of Mount Sirung (Figure 4).

The results of gravity data processing are correlated with Land Surface Temperature (LST) data and regional geological data to analyze the subsurface geothermal structure of Mount Sirung.

Figure 3. Research area (Google Earth, 2022).

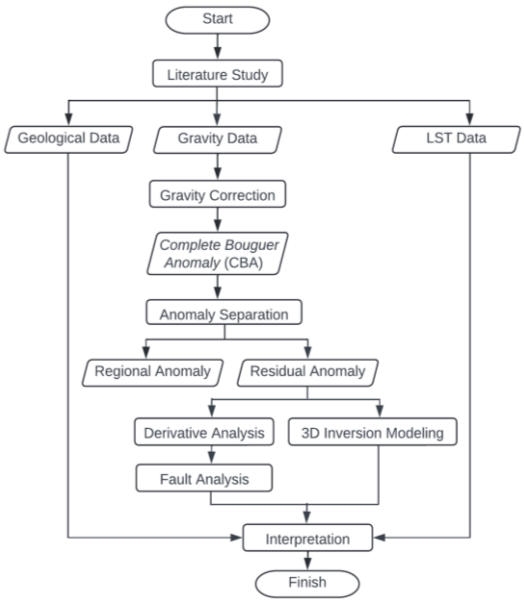

Figure 4. Research flowchart.

Results and Discussion

Complete Bouguer Anomaly (CBA) Map

Based on the results of the data processing, the complete Bouguer anomaly map (Figure 5) shows three different anomaly patterns. The low anomaly of 100.34 – 111.73 mGal is suspected as a lava interspersed with sandy tuff. The medium anomaly of 113.91 – 155.52 mGal is suspected as a breccia. The high anomaly of 157.29 – 170.87 mGal is suspected as a clay interspersed with breccia.

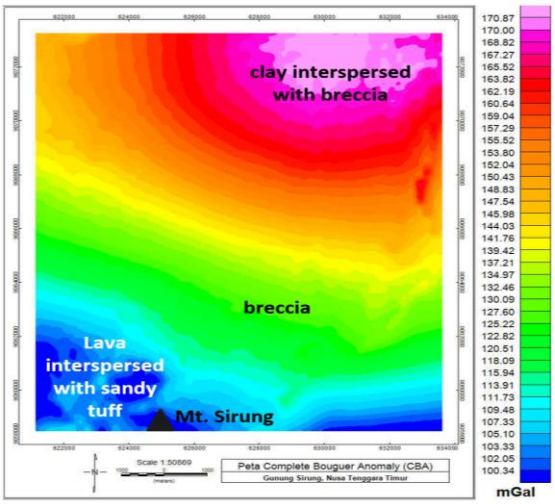

Figure 5. Complete Bouguer Anomaly (CBA) map.

Anomaly Separation

The contour of regional anomaly (Figure 6) is smoother than residual anomaly because it represents deep subsurface material, while residual anomaly represents shallow subsurface material. Separation of the anomalies is carried out with a Bandpass filter. Regional anomaly value ranges from 99.69 – 169.43 mGal.

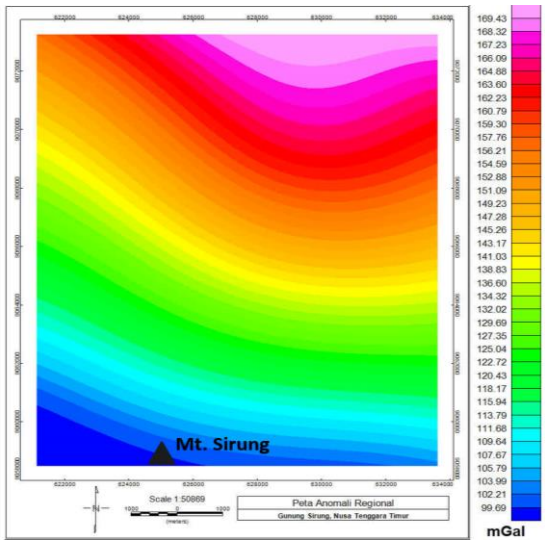

Figure 6. Regional anomaly map.

In the residual anomaly (Figure 7), low anomaly value of -5.07 – (-2.02) mGal is suspected as a lava interspersed with sandy tuff. The medium anomaly of -1.76 – 1.79 mGal is suspected as a breccia. The high anomaly of 1.97 – 5.22 mGal is suspected as a clay interspersed with breccia.

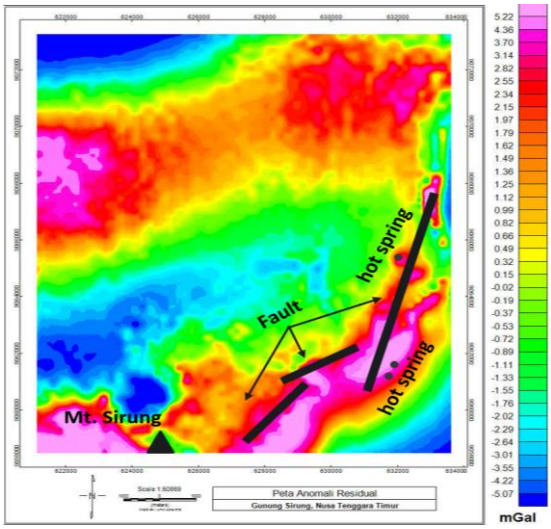

Figure 7. Residual anomaly map.

Land Surface Temperature (LST) Map

Geothermal potential can be recognized based on the distribution of surface temperature values that are higher than the surrounding area because surface temperature is associated with subsurface heat sources (Cahyono et al., 2019). Based on the results of overlaying the land surface temperature map (Figure 8) with the residual anomaly map, Mount Sirung has a surface temperature approximately 26.1 – 29.5°C. This area has a high temperature because there are manifestations of hot springs.

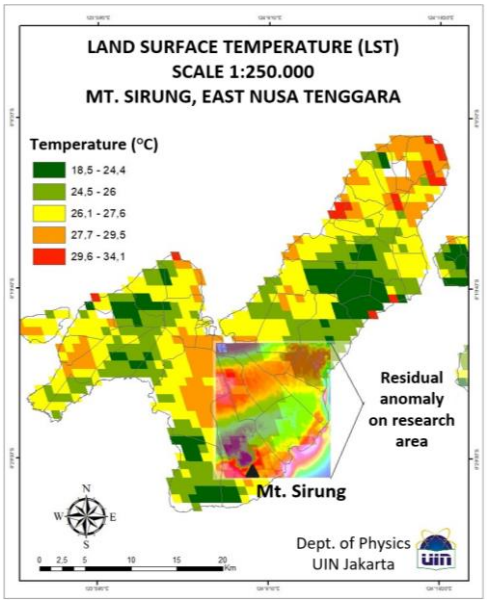

Figure 8. Land Surface Temperature (LST) map.

Derivative Analysis

Derivative analysis is carried out to determine the type of fault using the First Horizontal Derivative (FHD) (Figure 9) and Second Vertical Derivative (SVD) (Figure 10) methods by analyzing the maximum and minimum derivative values. The slicing trajectory is carried out in a northwest-southeast direction perpendicular to the main fault source (Figure 11). The main fault of Mount Sirung (Table 1 and Figure 12) is suspected to be at the contrast of low anomaly and high anomaly, which produces hot springs in the northeast and southwest directions (Koesoemadinata & Noya, 1969).

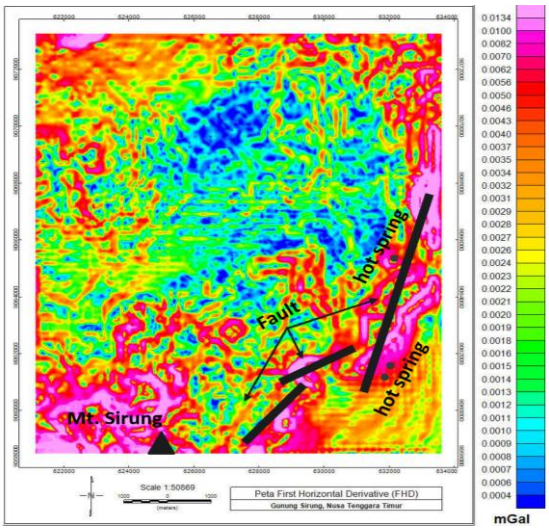

Figure 9. First Horizontal Derivative (FHD) map.

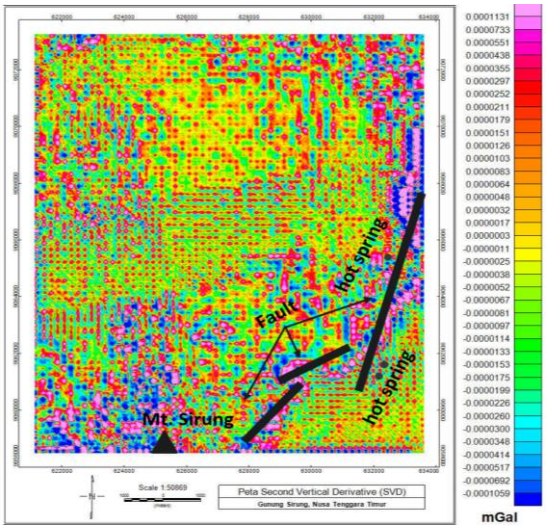

Figure 10. Second Vertical Derivative (SVD) map.

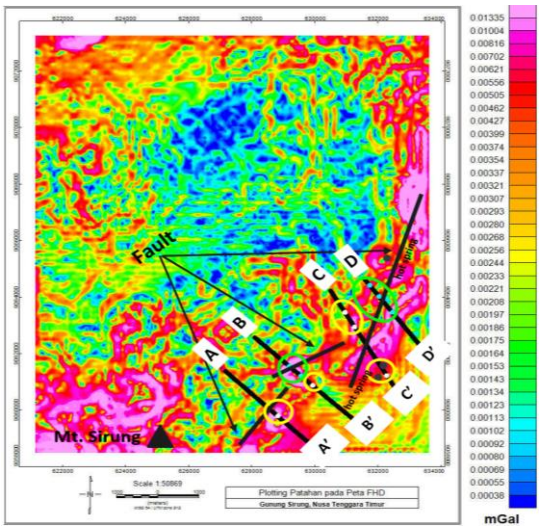

Figure 11. Fault plotting on First Horizontal Derivative (FHD) map.

Table 1. Fault analysis on Mount Sirung.

Line	Fault	Type	SVD		Coordinates	
			Max	Min	E	N
A-A'	P1	Reverse fault	1	3.1	628825.9	9059799.2
B-B'	P1	Normal fault	1	0.77	629194.8	9061560.5
	P2	Normal fault	1	0.69	629561.1	9061220.1
	P3	Reverse fault	0.12	0.27	629927.3	9060879.7
C-C'	P1	Reverse fault	0.04	0.14	630953.3	9063462.1
	P2	Reverse fault	0.16	0.32	631259.6	9062946.2
	P3	Reverse fault	0.14	0.53	632280.5	9061226.3
D-D'	P1	Normal fault	0.27	0.12	631733.5	9064423.6
	P2	Normal fault	0.6	0.09	632033.5	9064023.6
	P3	Normal fault	1	0.43	632453.5	9063463.6

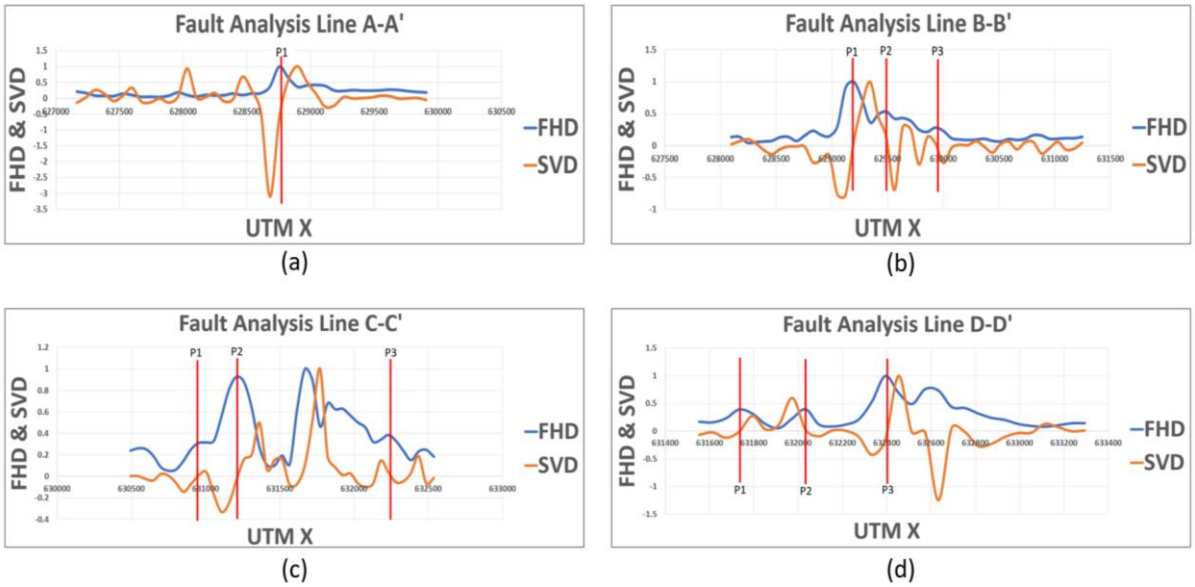

Figure 12. Fault analysis on Mount Sirung: (a) line A-A', (b) line B-B', (c) line C-C', (d) line D-D'.

3D Gravitational Inversion Modeling

Inversion modeling is used to identify the subsurface based on residual anomaly maps in three-dimensional form. This study consists of five slicing passes perpendicular to the main fault source (Figure 13–17).

The blue-green colored layer is suspected as a reservoir in the form of lava interspersed with sandy tuff with a low density of 1.98 – 2.03 g/cm^3. The white-yellow colored layer is suspected as a breccia with medium density of 2.16 – 2.21 g/cm^3. The red colored layer is suspected as a clay cap in the form of clay interspersed with breccia with high density of 2.34 – 2.39 g/cm^3.

Lava interspersed with sandy tuff has a large porosity that can store and drain large amounts of fluid. Clay interspersed with breccia is an impermeable layer, which can only store a limited amount of fluid because it has a small porosity (Darsono et al., 2017; Sugito et al., 2019).

Based on Table 2, the results of 3D gravitational inversion modeling show that there is agreement between the processed data and the theory. The low-density of Mount Sirung reservoir is located under a higher density clay cap as a trap for geothermal fluids (Sarkowi et al., 2021). The existence of geothermal manifestations can also be proven by the presence of hot springs (Figure 15) in the northeast of the study area (Koesoemadinata & Noya, 1969).

The presence of faults is characterized by the contrast of rock density between high density and low density. The fault will form a fracture to control fluid movement as the geothermal manifestation of Mount Sirung.

Isosurface is a representation of the value distribution of a material in three-dimensional form to see the distribution of each material (Sari et al., 2022). Top of reservoir modeling is depicted with an isosurface density of 2.19 g/cm^3. This modeling can show the distribution of lava interspersed with sandy tuff in the Gunung Sirung geothermal manifestation area (Figure 18).

Table 2. Depth analysis geothermal structure on Mount Sirung.

Line	Depth (m)	
	Reservoir (Lava interspersed with sandy tuff)	**Clay cap (Clay interspersed with breccia)**
L1 – L1’	600 – 1200	0 – 400
L2 – L2’	1000 – 1200	0 – 800
L3 – L3’	800 – 1400	0 – 600
L4 – L4’	700 – 1200	0 – 600
L5 – L5’	500 – 1400	0 – 400

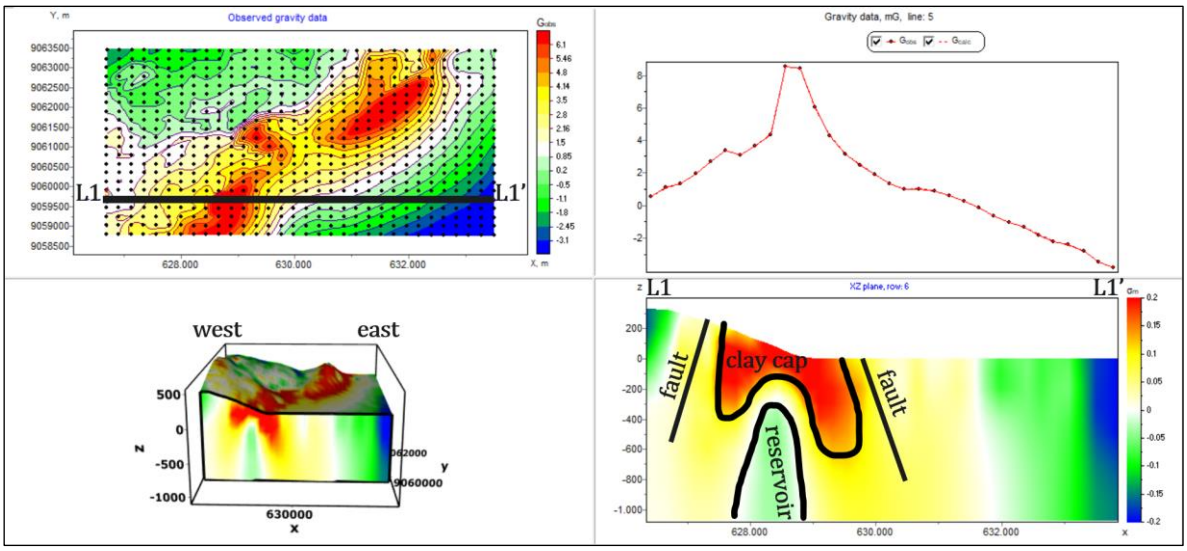

Figure 13. 3D gravitational inversion modeling line L1 – L1’ on Mount Sirung.

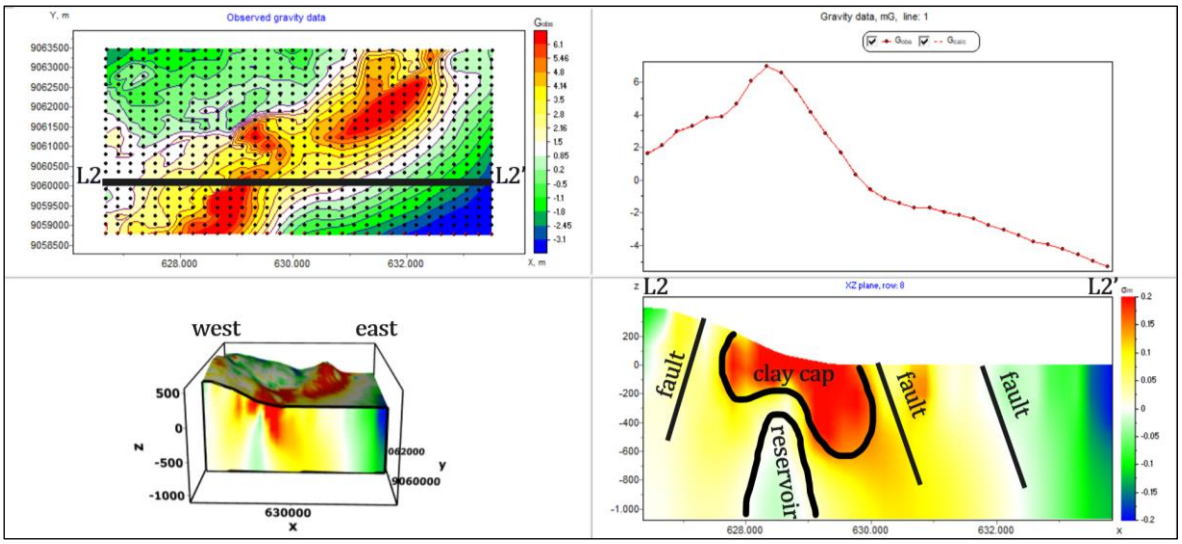

Figure 14. 3D gravitational inversion modeling line L2 – L2’ on Mount Sirung.

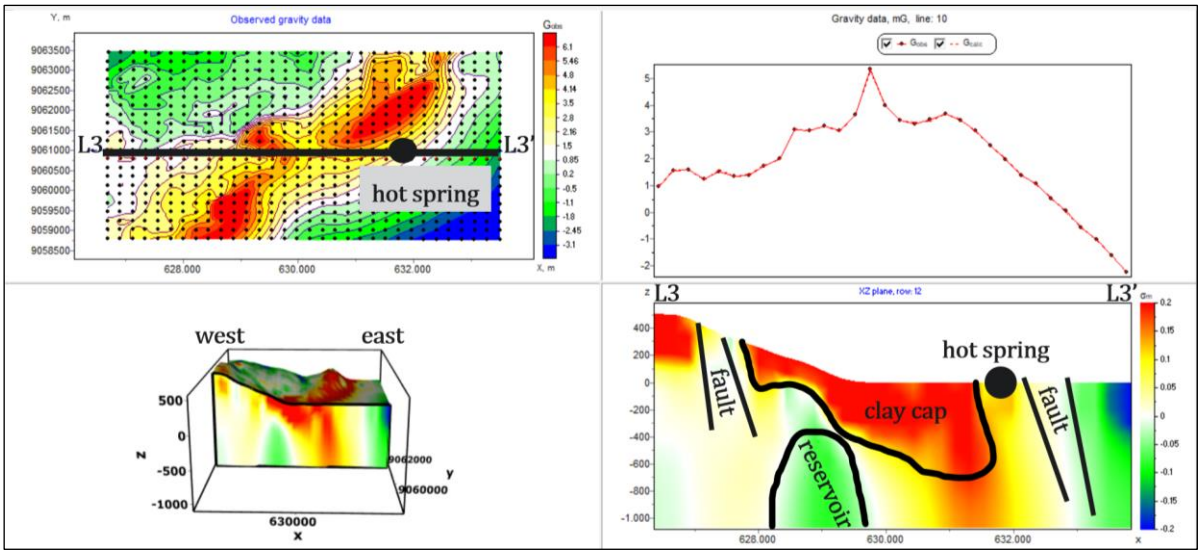

Figure 15. 3D gravitational inversion modeling line L3 – L3' on Mount Sirung.

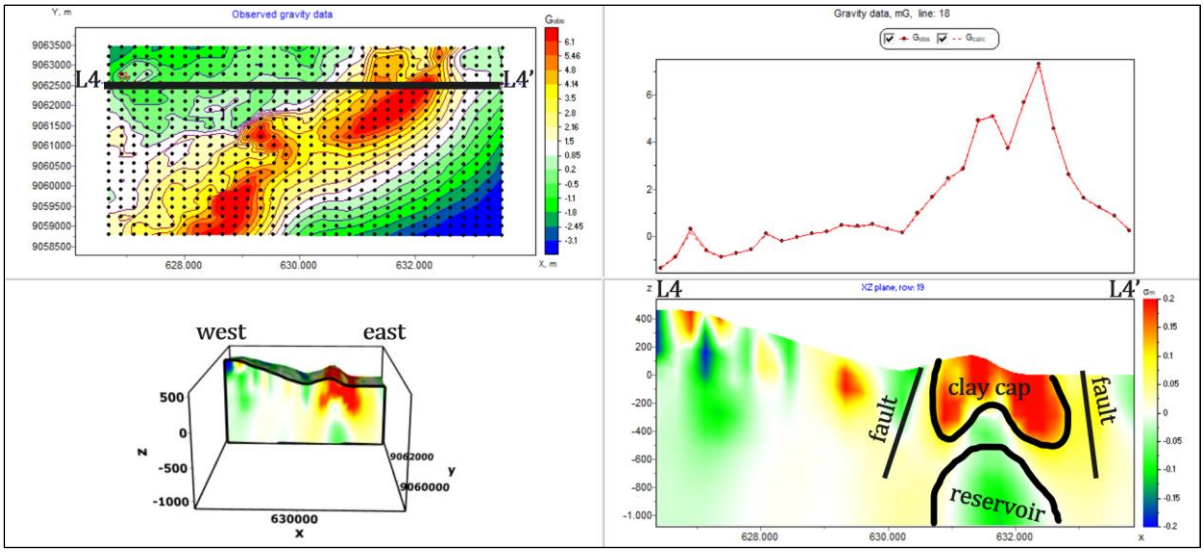

Figure 16. 3D gravitational inversion modeling line L4– L4' on Mount Sirung.

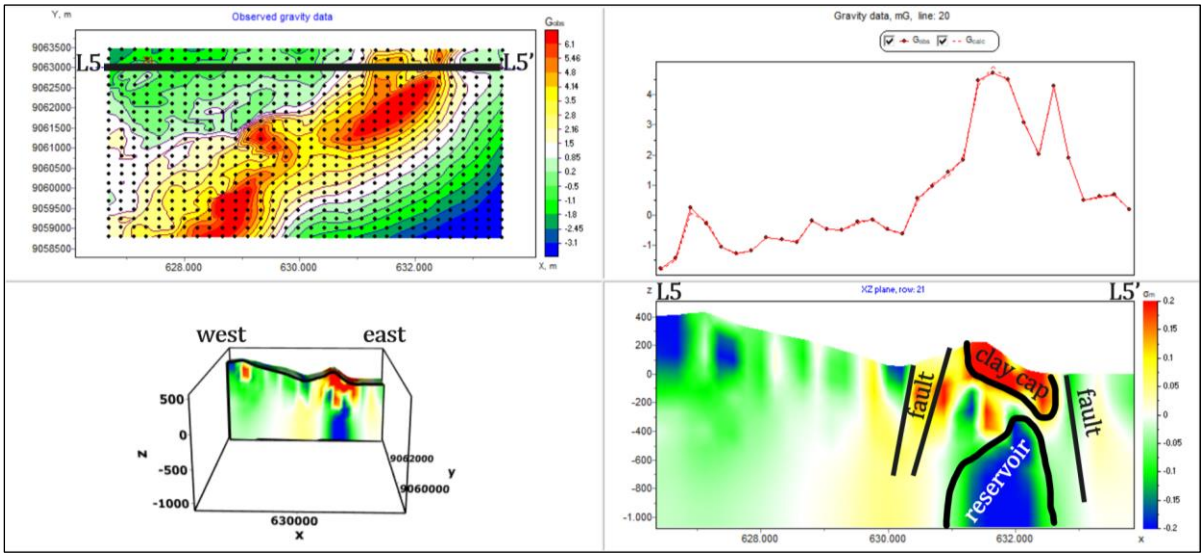

Figure 17. 3D gravitational inversion modeling line L5 – L5' on Mount Sirung.

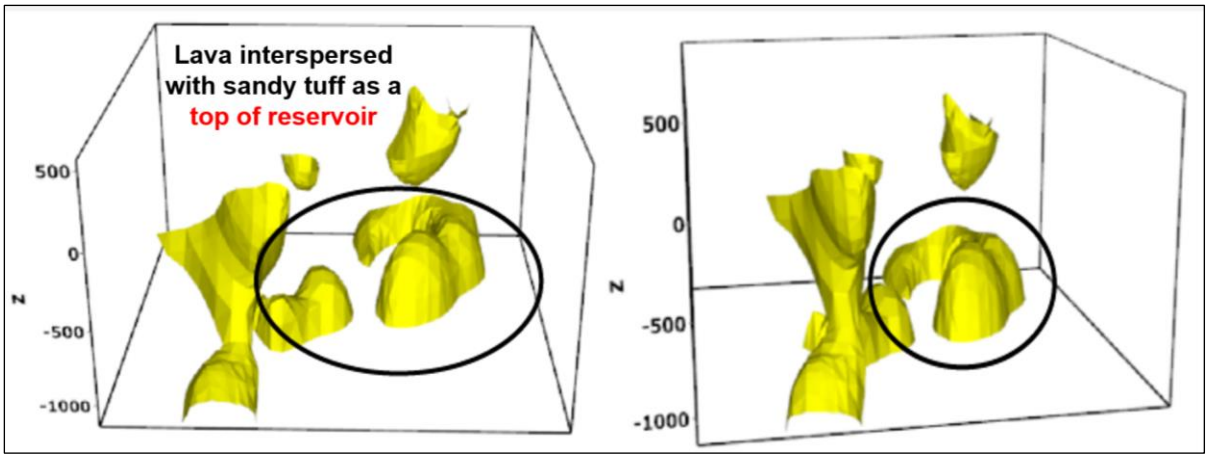

Figure 18. Isosurface top of reservoir on Mount Sirung.

Conclusion

Based on the Land Surface Temperature (LST) map, the research area at Mount Sirung has a surface temperature approximately 26.1 – 29.5°C, which is a high temperature because there are manifestations of hot springs.

Based on derivative analysis with the First Horizontal Derivative and Second Vertical Derivative methods, there are four trajectories with rising faults and normal faults as the geothermal control system of Mount Sirung in the northwest-southeast direction.

Based on 3D gravity inversion modeling, it is suspected that there are three types of rocks, which is clay interspersed with breccia as a clay cap with a density of 1.5 2.34 – 2.39 g/cm^3 at 0 – 600 m, and lava interspersed with sandy tuff as a reservoir with a density of 1.98 – 2.03 g/cm^3 at 700 – 1400 m.

Acknowledgements

The authors acknowledged PT Minelog Services Indonesia, GeoXplore Indonesia, and Syarif Hidayatullah State Islamic University Jakarta has providing facilities during the implementation of this research.

Author Contribution

Conception and data acquisition: NRP, DFF, and FRZ. Data interpretation and statistical analysis: AAP and NRP. Report writing publications: AAP. Performed the analysis: AAP, DFF, and FRZ. All authors reviewed the results and approved the final version of the manuscript.

Conflict of Interest

All authors have seen and agree with the contents of the manuscript and there is no financial interest to report. All authors certify that the submission is original work and is not under review at any other publication.

References

Ashat, A., Pratama, H. B., & Itoi, R. (2019). Updating conceptual model of Ciwidey-Patuha geothermal using dynamic numerical model. *IOP Conference Series: Earth and Environmental Science*, 254,012010. http://dx.doi.org/10.1088/1755-1315/254/1/012010

Cahyono, B. E., Jannah, N., & Suprianto, A. (2019). Analisis Sebaran Potensi dan Manifestasi Panas Bumi Pegunungan Ijen berdasarkan Suhu Permukaan dan Geomorfologi. *Natural B*, 5(1), 19–27. https://natural-b.ub.ac.id/index.php/natural-

b/article/view/452/

Darsono., Legowo, B., & Darmanto. (2017). Identifikasi Potensi Akuifer Tertekan berdasarkan Data Resistivitas Batuan (Kasus: Kecamatan Sambirejo Kabupaten Sragen). *Jurnal Fisika dan Aplikasinya*, 13(1), 34–38. http://dx.doi.org/10.12962/j24604682.v13i1.2151

Google Earth. (2022). *Research Location*. https://earth.google.com/web/search/GunungSirung

Gunawan, I., Windarta, J., & Harmoko, U. (2021). Overview Potensi Panas Bumi di Provinsi Jawa Barat. *Jurnal Energi Baru dan Terbarukan*, 2(2), 60–73. https://doi.org/10.14710/jebt.2021.11072

Hadi, M. N., & Kusnadi, D. (2015). Survei Geologi dan Geokimia Daerah Panas Bumi Pulau Pantar Kabupaten Alor, Provinsi Nusa Tenggara Timur. *Prosiding Hasil Kegiatan Lapangan Pusat Sumber Daya Geologi Tahun Anggaran*.

Hartini. (2020). Pemodelan Inversi Linier Least-Square (LS) pada Anomali Geomagnet Model Dyke. *Jurnal Hadron*, 2(2), 49–53. https://doi.org/10.33059/jh.v2i2.2689

Ibrahim, M. M., Utami, P., & Raharjo, I. B. (2022). Analisa Struktur Geologi berdasarkan Data Gravitasi Menggunakan Metode Second Vertical Derivative (SVD) Pada Lapangan Panas Bumi "X". *Jurnal Geosains dan Remote Sensing (JGRS)*, 3(2), 52–59. https://doi.org/10.23960/jgrs.2022.v3i2.76

Imran, P. B., Fernanda, E., & Sudrazat, S. D. (2021). Pengolahan Data Landsat dan Gravitasi Sebagai Indikasi Panasbumi Daerah Rana Kulan, NTT. *Jurnal Geofisika Eksplorasi*, 7(1), 41–51. https://doi.org/10.23960/jge.v7i1.10

Koesoemadinata, S., & Noya, N. (1969). *Geological Map of Lomblen Quadrangle, East Nusa Tenggara Scale 1:250.000*. Pusat Penelitian dan Pengembangan Geologi.

Luthfi, M., Haryanto, A. D., Hutabarat, J., & Siagian, H. (2020). Pemodelan Sistem Panasbumi pada Sumur ML-1, ML-2 dan ML-3 berdasarkan Analisis Petrografi dan Magnetotellurik di Lapangan Panasbumi Sorik Marapi, Kabupaten Mandailing Natal, Sumatera Utara. *Geoscience Journal*, 4(2), 154–162. http://jurnal.unpad.ac.id/geoscience/article/view/29089

Ministry of Energy and Mineral Resources. (2017). *Potensi Panas Bumi Indonesia Jilid 2*. Badan Geologi.

Ministry of Energy and Mineral Resources. (2021). *Triwulan III 2021: Rasio Elektrifikasi 99,40%, Kapasitas Pembangkit EBT 386 MW*. Siaran Pers Indonesia. https://ebtke.esdm.go.id/post/2021/11/22/3013/triwulan.iii.2021.rasio.elektrifikasi.9940.kapasitas.pembangkit.ebt.386.mw

Permana, N. R., Gunawan, B., Primastika, A. A., & Novitasari, D. (2022). Characteristics of Palu-Koro Fault based on Derivative Analysis and Euler Deconvolution Model of Gravity Data. *Journal of Physics: Conference Series*, 2377, 012041. https://doi.org/10.1088/1742-6596/2377/1/012041

Permana, N. R., Gunawan, B., Primastika, A. A., Shafa, D., Fadrian, D. F., & Zani, F. R. (2022b). Identification of Alteration Zone and Gold Mineralization based on Magnetic Anomaly and 3D Model of Geomagnetic Satellite Data Inversion of Mount Pongkor Area, West Java. *Journal of Natural Sciences and Mathematics Research*, 8(2), 94–102. https://doi.org/10.21580/jnsmr.2022.8.2.13177

Rahadinata, T., Takodama, I., & Zarkasyi, A. (2019). Penerapan Koreksi Topografi pada Data Magnetotellurik dan Analisis Data Gaya Berat dalam

Interpretasi Daerah Panas Bumi Pantar, Kabupaten Alor, Provinsi Nusa Tenggara Timur. *Buletin Sumber Daya Geologi*, 14(3), 156–168. https://doi.org/10.47599/bsdg.v14i3.290

Rey, R. B. & Poluakan, C. (2020). Identifikasi mineral batuan pada daerah manifestasi mata air panas di Koya Kecamatan Tondano Selatan Kabupaten Minahasa menggunakan sem-edx dan ftir. *Jurnal Fisika dan Terapannya*, 1(1), 12–16. https://eurekaunima.com/index.php/fista/article/view/57/29

Reynolds, J. M. (1997). *An Introduction to Applied and Environmental Geophysics.* John Wiley and Sons.

Salam, R. A., Harmoko, U., & Yulianto, T. (2017). Pemodelan 2D sistem panas bumi daerah Garut bagian timur menggunakan metode magnetotellurik. *Youngster Physics Journal*, 6(2), 143–150. https://ejournal3.undip.ac.id/index.php/bfd/article/view/17118

Saptadji, N. (2001). *Teknik Panas Bumi.* Bandung Institute of Technology Press.

Sari, H. P., Suprianto, A., & Priyantari, N. (2022). Groundwater Distribution and Potency in Faculty of Mathematics and Natural Science, Universitas Jember based on 3-Dimensional Resistivity Data Modeling. *Jurnal Berkala Saintek*, 10(1), 32–36. https://doi.org/10.19184/bst.v10i1.23025

Sarkowi, M., Sawitri, R. F., Mulyanto, B. S., & Wibowo, R. C. (2021). Wai Selabung geothermal reservoir analysis based on gravity method. *Jurnal Ilmiah Pendidikan Fisika Al-BiRuNi*, 10(2), 211–229. https://doi.org/10.24042/jipfalbiruni.v10i2.9705

Sehah., Prabowo, U. N., & Raharjo, S. A. (2021). Pemanfaatan Data Anomali Gravitasi Citra Satelit untuk Interpretasi Kualitatif Batas Cekungan Air Tanah Purwokerto-Purbalingga. Prosiding Seminar Nasional dan Call for Papers. http://jurnal.lppm.unsoed.ac.id/ojs/index.php/Prosiding/article/viewFile/1841/1600

Sidik, I. F., Susilo, A., & Sulastomo, G. (2014). Identifikasi Sesar Di Daerah Pongkor Bogor Jawa Barat Dengan Menggunakan Metode Gayaberat. *Brawijaya Physics Student Journal*, 2(1), 21–25. http://physics.studentjournal.ub.ac.id/index.php/psj/article/view/125

Sugianto, A., Takodama, I., & Rahadinata, T. (2017). Identification of Pantar Geothermal Structures Derived from Gradient Horizontal Analysis and 3D Modeling of Gravity Data. *Buletin Sumber Daya Geologi*, 12(2), 135–143.

Sugita, M. I., Janah, A. F., Rahmawati, D., Supriyadi., & Khumaedi. (2020). Analisis Data Gaya Berat di Daerah Bendan Duwur Semarang. *Journal of Research and Technology*. 6(1), 81–90. https://journal.unusida.ac.id/index.php/jrt/article/view/143/152

Sugito., Hartono., Irayani, Z., & Abdullatif, R. F. (2019). Eksplorasi potensi akuifer menggunakan metode geolistrik resistivitas di desa plana Kec. Somagede Kab. Banyumas. *Prosiding Seminar Nasional LPPM Unsoed*, 9(1), 12–22. http://jurnal.lppm.unsoed.ac.id/ojs/index.php/Prosiding/article/viewFile/1102/956

Wachidah, N. & Minarto, E. (2018). Identifikasi Struktur Lapisan Bawah Permukaan Daerah Potensial Mineral dengan Menggunakan Metode Gravitasi di Lapangan "A", Pongkor, Jawa Barat. *Jurnal Sains dan Seni ITS*, 7(1), B32–B37. http://dx.doi.org/10.12962/j23373520.v7i1.28673

Yudha, S. W., Tjahjono, B., & Longhurst, P. (2022). Unearthing the Dynamics of

Indonesia's Geothermal Energy Development. *Energies*, 15(14), 5009. https://doi.org/10.3390/en15145009

Yulistina, S. (2018). Studi Identifikasi Struktur Geologi Bawah Permukaan untuk Mengetahui Sistem Sesar berdasarkan Analisis First Horizontal Derivative (FHD), Second Vertical Derivative (SVD), dan 2,5D Forward Modeling di Daerah Manokwari Papua Barat. *Jurnal Geofisika Eksplorasi*, 4(2), 173–186. http://dx.doi.org/10.23960/jge.v4i2.15